Towards Robust Multimodal Land Use Classification: A Convolutional Embedded Transformer

Muhammad Zia Ur Rehman[1][a], Syed Mohammed Shamsul Islam[1][b], Anwaar UlHaq[2][c],
David Blake[1][d] and Naeem Janjua[3][e]
[1]*School of Science, Edith Cowan University, Australia*
[2]*School of Engineering and Technology Centre for Intelligent Systems, Central Queensland University, Australia*
[3]*College of Science and Engineering, Flinders University, Australia*
{*m.ziaurrehman, syed.islam, d.blake*}*@ecu.edu.au, a.anwaarulhaq@cqu.edu.au, naeem.janjua@flinders.edu.au*

Keywords: Land Use Classification, Multimodal, Transformer, Cross-Modal Learning.

Abstract: Multisource remote sensing data has gained significant attention in land use classification. However, effectively extracting both local and global features from various modalities and fusing them to leverage their complementary information remains a substantial challenge. In this paper, we address this by exploring the use of transformers for simultaneous local and global feature extraction while enabling cross-modality learning to improve the integration of complementary information from HSI and LiDAR data modalities. We propose a spatial feature enhancer module (SFEM) that efficiently captures features across spectral bands while preserving spatial integrity for downstream learning tasks. Building on this, we introduce a cross-modal convolutional transformer, which extracts both local and global features using a multi-scale convolutional embedded encoder (MSCE). The convolutional layers embedded in the encoder facilitate the blending of local and global features. Additionally, cross-modal learning is incorporated to effectively capture complementary information from HSI and LiDAR modalities. Evaluation on the Trento dataset highlights the effectiveness of the proposed approach, achieving an average accuracy of 99.04% and surpassing comparable methods.

1 INTRODUCTION

The use of remote sensing in land use classification is necessary for effective environmental management, urban planning, or precision agriculture. It is one of the critical tasks that leads to the execution of management plans through remote sensing technology. Over the last decade, hyperspectral imaging (HSI) has been widely used for land use classification that has the ability to capture spectral information (Hong et al., 2021) (Ghamisi et al., 2017). This allows HSI to distinguish between different objects on the ground using their unique spectral signatures. However, HSI faces challenges in distinguishing objects that share similar spectral signatures but different spatial structures, reducing its effectiveness in diverse landscapes.

The recent technological advancements in remote sensing systems have significantly enhanced the possibilities of gathering multimodal remote sensing data (Gómez-Chova et al., 2015). The utilization of multimodal data has already proved its significance for classification tasks in different fields (Tang et al., 2022) (Ding et al., 2021) (Hermessi et al., 2021). These advancements have shifted research towards the multimodal domain in this field as well, where integration of HSI with other imaging modalities such as LiDAR provides complementary information in terms of height (Ding et al., 2022), thereby improving classification abilities of objects on the ground facilitating precise and effective management and planning. However, effective fusion of modalities is a current challenge along with feature extraction.

Traditional classification techniques, employed in the early stages of research within this domain (Liao et al., 2014), provide a baseline for further research advancements. However, the complexity of HSI data and the limitations associated with shallow feature extraction reduces their effectiveness. Recently, convolutional neural networks (CNNs) have been widely recognized in land use classification due to their dis-

[a] https://orcid.org/0000-0001-9531-1941
[b] https://orcid.org/0000-0002-3200-2903
[c] https://orcid.org/0000-0002-5145-7276
[d] https://orcid.org/0000-0003-3747-2960
[e] https://orcid.org/0000-0003-0483-8196

Rehman, M. Z. U., Islam, S. M. S., UlHaq, A., Blake, D. and Janjua, N.
Towards Robust Multimodal Land Use Classification: A Convolutional Embedded Transformer.
DOI: 10.5220/0013191300003912
Paper published under CC license (CC BY-NC-ND 4.0)
In *Proceedings of the 20th International Joint Conference on Computer Vision, Imaging and Computer Graphics Theory and Applications (VISIGRAPP 2025) - Volume 3: VISAPP*, pages 143-153
ISBN: 978-989-758-728-3; ISSN: 2184-4321
Proceedings Copyright © 2025 by SCITEPRESS – Science and Technology Publications, Lda.

criminative feature extraction capabilities (Xue et al., 2021) (Du et al., 2021) (Zhang et al., 2021). Furthermore, encoder-decoder based architectures such as EndNet (Hong et al., 2020) and CCR-Net (Wu et al., 2021) have been employed to enhance feature extraction and the fusion of modalities, with their strength lying in their compact architecture that facilitates efficient data processing and integration. Although these techniques are good at extracting local features, they lack global context and semantics among pixels (Hong et al., 2021). To fill this gap, various studies have integrated additional attention-based modules with CNNs, which have demonstrated better performance over conventional CNN-based models (Feng et al., 2021) (Mohla et al., 2020). Despite these advancements in CNN-based framework challenges persists in finding global and long-range feature dependencies (Hong et al., 2022).

Vision Transformer (ViT), a variant of the transformer developed for natural language processing (NLP) tasks, has emerged as a potential solution to address limitations in extracting global information through its unique self-attention mechanism (Vaswani, 2017). Similar to conventional transformers, ViT generates patches and through its self-attention mechanism, it attends each patch to facilitate finding global correlations among them. Several transformer-based techniques are proposed to improve its feature extracting capabilities. However, transformers struggle to capture local information and features. To address this limitation, CNNs are being integrated with transformers to complement and enhance their ability to process local details (Yu et al., 2022) (Zhang et al., 2022), which shows improvements. However, current studies lack interaction between local and global features that could provide better semantic information, thus potentially improving the performance.

To address this shortcoming, a transformer model is proposed with a convolutional block embedded in the encoder of the transformer. The embedded convolutional block contributes towards capturing local features, whereas the conventional transformer's multi-head self-attention (MHSA) captures global features. Therefore, the proposed model has the capability to capture both local and global features. Moreover, it facilitates the interaction of local and global features within the transformer, thus providing enriched semantic information, which as a result improves classification accuracy. The main contributions of this study are as follows:

1. A spatial feature enhancer module (SFEM) is proposed to preserve spatial information for subsequent processing while enriching the spectral feature set.
2. A transformer model is proposed for HSI and LiDAR land use classification with a transformer encoder that consists of a multiscale convolution block, enabling the simultaneous extraction of local and global features.
3. A cross-modal attention module is employed for the feature interaction between HSI and LiDAR modalities that help learn complementary information.

Several land use classification techniques are discussed in Section 2. Section 3 discusses the detailed methodology of the proposed technique. Experimental results are presented in Section 4 while Section 5 concludes the study.

2 RELATED WORK

Effective land use classification remains a challenge due to the heterogeneous nature of land. Researchers have proposed several techniques to address the challenges associated with land use classification. Over time, many traditional and deep learning-based techniques for land use classification have been proposed. Traditional techniques utilized filter and profile-based approaches. In filter-based techniques, morphological and Gabor filters are commonly used for feature extraction (Jia et al., 2021) (Rasti and Ghamisi, 2020). On the other hand, profile-based techniques are combinations of various filters that are used together to extract features. Morphological attribute profiles (Liao et al., 2014) and extinction attribute profiles (Rasti et al., 2017b) were commonly used. After extracting features using the aforementioned techniques, features are either stacked together and classified using different classifiers such as support vector machines (SVM) and random forest (RF) or classifiers are applied independently, with the final decision being made through a voting-based decision strategy.

Recently, deep learning-based techniques have overtaken traditional methods due to their superior feature extraction capabilities and are extensively used for land use classification. Generally, dual-stream frameworks are proposed (Feng et al., 2019), which include encoder-decoder-based architectures as well. EndNet (Hong et al., 2020) and CCR-Net (Wu et al., 2021) both follow the encoder-decoder architecture; for the mutual exchange of information between modalities, reconstruction-based fusion strategies are adopted. Some proposed techniques are composed of triple streams (Feng et al., 2019) (Li et al., 2022), primarily to process modalities differently to extract spatial-spectral features from them. Some advanced techniques utilize attention mechanisms along with CNNs to extract robust features. (Mohla et al., 2020) proposed FusAtNeT, one of the initial attention-based techniques employed for land use classification. Specialized spatial and spectral attention modules have been used along with CNN-based feature extractors; the incorporation of attention modules showed improved classification performance. Similarly, (Wang et al., 2022) proposed modality-specific attention modules to highlight important features. To integrate features of different modalities, a modality attention (MA) module is proposed that provides better feature interaction between modalities compared to traditional early and late fusion strategies. (Fan et al., 2022) proposed composite attention followed by self-calibrated convolution that can extract multiscale features. To preserve the complementary information of modalities, an attention-based feature fusion (FF) module is employed that adaptively fuses heterogeneous features. These techniques have significantly improved classification performance; yet, they do not adequately handle the voluminous spectral information in HSI data due to the intrinsic limitations of CNNs. This limitation results in pixels with minor spectral differences not being effectively distinguishable. Transformers, with their capability to process sequential data, could effectively distinguish between these pixels in spectral data.

(Ni et al., 2024) proposed a multiscale head selection transformer network with a hierarchical convolutional feature extraction module. Features are extracted independently from both modalities and combined together before further processing through multiscale 2D convolutional layers and a conventional transformer. Finally, a classification decision is performed using a CNN and transformer-based class token. (Zhang et al., 2023) proposed a transformer and multiscale fusion network for joint HSI and LiDAR classification. Initially, it extracts multiscale features from both modalities using multiscale attention. Subsequently, the extracted features are fused together using transformer-based attention calculation. Later on, the multiscale and fused features are classified using a specially designed multi-output module. (Roy et al., 2023) introduced a multimodal fusion transformer for classifying HSI and LiDAR data. In their approach, LiDAR data is utilized as a learnable token, combined with HSI tokens for feature learning. However, this method does not completely integrate the valuable information from both modalities, which consequently restricts the potential accuracy of the classification. In addition to these, several transformer-based techniques have been proposed for land use classification (Roy et al., 2024) (Yang et al., 2024). Despite these advancements, challenges still persist in the effective interaction between local and global features during the feature learning process and their fusion, which is crucial for capturing the distinctive characteristics arising from subtle differences in land cover types.

3 METHODOLOGY

In this study, a new transformer-based model is proposed for multimodal land use classification that is capable of extracting local and global features simultaneously. The framework of the proposed technique is presented in Figure 1 and described in the following subsections. Subsection 3.1 explains the preprocessing steps, while Subsection 3.2 describes shallow feature extraction and tokenization required for the transformer model to further process the features. Subsection 3.3 discusses the proposed cross-modal convolutional transformer.

3.1 Pre-Prossessing

The original HSI data can be denoted as $X_H \in \mathbb{R}^{H\times W\times D}$, and LiDAR data can be represented as $X_L \in \mathbb{R}^{H\times W}$. The spatial dimensions—height and width—are represented by H and W, respectively, while D represents the spectral dimensions of the HSI data. HSI data has redundant spectral information within hundreds of spectral dimensions. Therefore, principle component analysis (PCA) is used to select informative spectral bands of the original HSI data. The HSI data with reduced spectral dimensions is then represented as $X_H \in \mathbb{R}^{H\times W\times D_{\text{red}}}$, where D_{red} is 30. Both the HSI and LiDAR data are further processed; padding is applied to preserve edge information, and patches of dimension $S\times S$, where S is 11, are generated. The center pixel of each patch represents the class label. The resulting HSI and LiDAR data is represented as $X_H^P \in \mathbb{R}^{S\times S\times D_{\text{red}}}$ and $X_L^P \in \mathbb{R}^{S\times S\times 1}$, respectively.

3.2 Spatial Feature Enhancer Module and Tokenization

In this study, we propose a convolution-based spatial feature enhancer module (SFEM) for initial feature extraction. This module utilizes pointwise convolutions, which are particularly important for HSI data characterized by rich spectral information at each spatial location. Pointwise convolutions facilitate the learning of inter-band dependencies among different spectral bands, a critical aspect in HSI where corre-

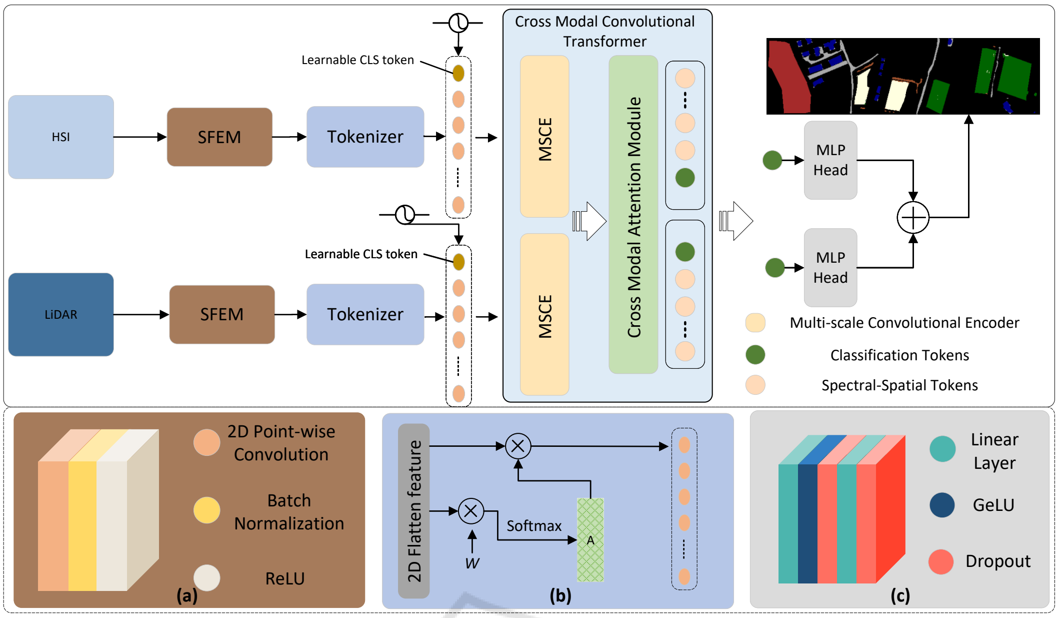

Figure 1: The proposed framework for land use classification using HSI and LiDAR modalities. The internal architecture of the spatial feature enhancer module (SFEM) is shown in (a), the tokenizer is presented in (b), and the internal architecture of the multi-layer perceptron (MLP) head is shown in (c).

lations between different spectral bands aid in understanding complex patterns within the data. Though pointwise convolutions do not extract spatial features directly, the enriched spectral features they produce can indirectly enhance spatial features for subsequent processing. Our motivation is to preserve spatial details while providing a rich feature set to downstream modules, enabling more effective and sophisticated feature learning. The pointwise convolutions apply a 1×1 kernel to each spatial location, preserving the original spatial dimensions of the data. This approach enhances the overall framework's capability to process and synthesize the information across channels without distorting the spatial information, unlike techniques (Roy et al., 2023) (Roy et al., 2024) that do not preserve the spatial information due to the use of large kernel sizes in convolution layers. The pointwise convolution layers in the SFEM are followed by batch normalization and a rectified linear unit (ReLU) layer to stabilize the learning process and introduce necessary non-linearity, respectively. The architecture of SFEM is shown in Figure 1(a).

Initial feature extraction is performed through the SFEM for both HSI and LiDAR modalities. For subsequent processing of these extracted features in the classification task through the transformer module, tokenization is necessary. This tokenization is performed by a tokenizer shown in Figure 1(b), which converts feature maps into vectors by flattening them. The 2D flattened feature map for HSI is represented as $X_H^{flat} \in \mathbb{R}^{xy \times z_h}$, and similarly, flattened LiDAR features are represented as $X_L^{flat} \in \mathbb{R}^{xy \times z_l}$, where x denotes the height, y the width, and z_h, z_l the number of spectral bands for HSI and LiDAR, respectively. The tokenization process employs two separate learnable weights W_1 and W_2, one for each modality, with weights initialized using a normal distribution through Xavier initialization (Zhao et al., 2022). These weights are pointwise multiplied with feature maps and softmax is applied to convert its scores. The output is then transposed and multiplied with a 2D flattened feature map. The tokenization process results in high-level semantic tokens of HSI and LiDAR. The process of tokenization HSI data is mathematically expressed as follows:

$$x^{hsi} = \mathrm{softmax}(X_H^{flat} W_1)^T X_H^{flat} \tag{1}$$

3.3 Cross-Modal Convolutional Transformer

The proposed cross-modal convolutional transformer consists of two parts: a multiscale convolutional embedded encoder and a cross-modal attention module. Subsubsection 3.3.1 provides a detailed discussion of the encoder, while Subsubsection 3.3.2 discusses cross-modal attention module for cross-modal feature learning and the final classification.

3.3.1 Multi-Scale Convolution Embedded Encoder

The semantic tokens generated by the tokenizer are utilized by the transformer encoder to identify correlations between tokens through a multi-head self-attention mechanism, which comprises multiple self-attention mechanisms. Each self-attention mechanism computes correlations between tokens using three learnable weights: W_q for queries, W_k for keys, and W_v for values. These weights are multiplied with the feature tokens and projected onto three linearly mapped matrices: Q for queries, K for keys, and V for values. Using Q and K, attention scores are then computed with the softmax function. The self-attention is mathematically represented as follows:

$$\mathrm{SA} = \mathrm{Attention}(Q,K,V) = \mathrm{softmax}\left(\frac{QK^T}{\sqrt{D}}\right)V \quad (2)$$

In the case of multi-head self-attention, the projection of tokens is divided by the number of heads, i.e., $D = \frac{C}{h}$, where h is the number of heads. However, after concatenation, the dimensions are restored by applying a projection matrix W^O to combine the outputs from all heads back to the original dimensionality, ensuring that the multi-head self-attention effectively integrates diverse perspectives from each head. The multi-head self-attention is represented in Equation 3.

$$\mathrm{MHSA}(Q,K,V) = \mathrm{Concat}(\mathrm{SA}_1, \mathrm{SA}_2, \ldots, \mathrm{SA}_h)W^O \quad (3)$$

where $\mathrm{SA}_i = \mathrm{softmax}\left(\frac{Q_i K_i^T}{\sqrt{d_k}}\right)V_i$ represents the output from the i-th self-attention head, Q_i, K_i, and V_i are parts of Q, K, and V that correspond to the i-th head, and W^O is the output projection matrix that recombines the attention outputs into a single tensor. The MHSA computes correlations in a global manner but lacks correlation between local semantic tokens.

To address this issue, inspired by (Gulati et al., 2020), a convolutional block is embedded in the transformer encoder after the multi-head self-attention to find correlations between local tokens from those already processed through MHSA. The architecture of the MSCE is shown in Figure 2. The adapted convolution block (Khotimah et al., 2023) starts with the pointwise convolution followed by dual stream 1D convolutions that find correlations between tokens at different scales for local semantics. These streams utilize 1D dilated convolutions with kernel sizes of 3 and 5. Subsequently, batch normalization and a swish activation function are applied. To enrich local semantics further, the outputs of both convolutions are merged using element-wise summation. Finally, the merged output is passed through a pointwise convolution again to transform the features back to their original size. The convolutional block is sandwiched between two feed-forward networks. Residual connection has also been used to avoid the vanishing gradient problem.

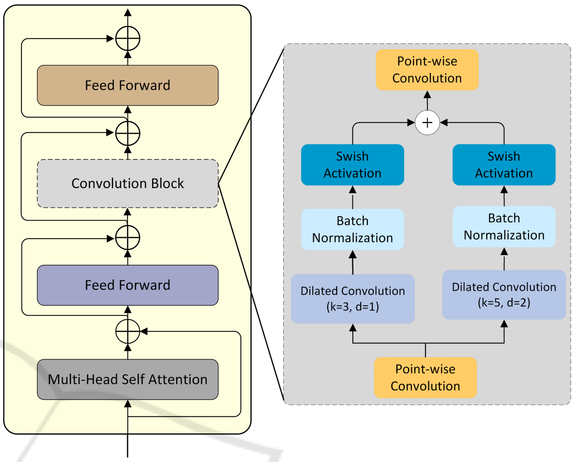

Figure 2: The architecture of the multi-scale convolutional embedded encoder (MSCE). The left shows the transformer encoder embedded with a convolutional block, while the right shows the internal layer structure of the convolutional block.

3.3.2 Cross-Modal Feature Learning and Classification

As both modalities have been treated separately thus far, capturing information specific to their corresponding modality, it is important to learn complementary details from each other. Cross learning can improve the learning capability of the model to effectively utilize complementary information for final classification (Chen et al., 2021), (Xue et al., 2022).

In the proposed cross-modal feature learning strategy, classification tokens containing rich information specific to each modality are exchanged between modalities to learn the complementary information present in each. In this process, the HSI classification token attends to all LiDAR tokens, and the LiDAR classification token attends to all HSI tokens. After this exchange of information, classification tokens are projected back to their respective modalities, but now these classification tokens contain complementary information from the other modality. These updated classification tokens interact with their own tokens in the next encoder, thus passing learned information from the other modality and this interaction further enriches the exchange of information. For simplicity and to avoid confusion, we have explained the cross-modal feature learning for HSI. This process is also illustrated in Figure 3. As we know, LiDAR tokens are of two types: feature tokens and classification (cls) tokens. The cls token of LiDAR is replaced with the HSI cls token. This gives a new set of tokens that we call cross-modal tokens. Mathematically, the new set of feature tokens is shown in Equation 4.

$$X_{\text{ct}}^{hsi} = [f^l(x_{\text{cls}}^{hsi'}) \parallel x^{lidar}], \tag{4}$$

where $f^l(\cdot)$ is the linear transformation on the HSI cls token for dimensionality alignment. Subsequently, cross-attention is performed between $x_{\text{cls}}^{hsi'}$ and X_{ct}^{hsi}. The cls token ($x_{\text{cls}}^{hsi'}$) is the query used for cross-attention that contains information of the HSI feature tokens. The cross-attention is mathematically represented as follows:

$$\begin{gathered} q = x_{\text{cls}}^{\text{hsi}'} W_q, \quad k = X_{\text{ct}}^{\text{hsi}} W_k, \quad v = X_{\text{ct}}^{\text{hsi}} W_v, \\ \mathbf{A} = \text{softmax}\left(\frac{qk^T}{\sqrt{C/h}}\right), \quad \text{CA}(X_{\text{ct}}^{\text{hsi}}) = \mathbf{A}v \end{gathered} \tag{5}$$

Where W_q, W_k, and W_v are learnable weights. Similar to self-attention, multiple heads have been used for cross-attention. The multi-head cross-attention is mathematically shown in Equation 6. The output of cross-attention is shown in Equation 7.

$$y_{\text{cls}}^{hsi} = f^l(x_{\text{cls}}^{hsi}) + \text{MHCA}(\text{LN} f^l(x_{\text{cls}}^{hsi}) \parallel x_{\text{ft}}^{lidar})) \tag{6}$$

$$z^{hsi} = [g^l(y_{\text{cls}}^{hsi}) \parallel x_{\text{ft}}^{hsi}] \tag{7}$$

The HSI classification token (y_{cls}^{hsi}) and LiDAR classification token (y_{cls}^{lidar}), obtained by the process discussed above, are passed through a linear transformation layer $g^l(\cdot)$ as shown in Figure 3. Following that, these tokens passed through two separate MLP heads, as depicted in Figure 1. Each MLP head is composed of two linear layers, a GeLU activation, and a dropout layer. The last linear layer employs softmax activation. The arrangement of MLP layers is shown in Figure 1 (c). The outputs of both MLP heads are added together for the final classification.

4 EXPERIMENTAL DETAILS AND RESULTS

This section presents the results obtained using the proposed technique. The dataset employed for evaluation is discussed in Subsection 4.1, while the experimental setup is defined in Subsection 4.2. Subsection 4.3 presents the classification results, including comparisons with other techniques, to demonstrate the effectiveness of the proposed approach. Subsection 4.4 discusses the ablation study to further evaluate the impact of different parameters.

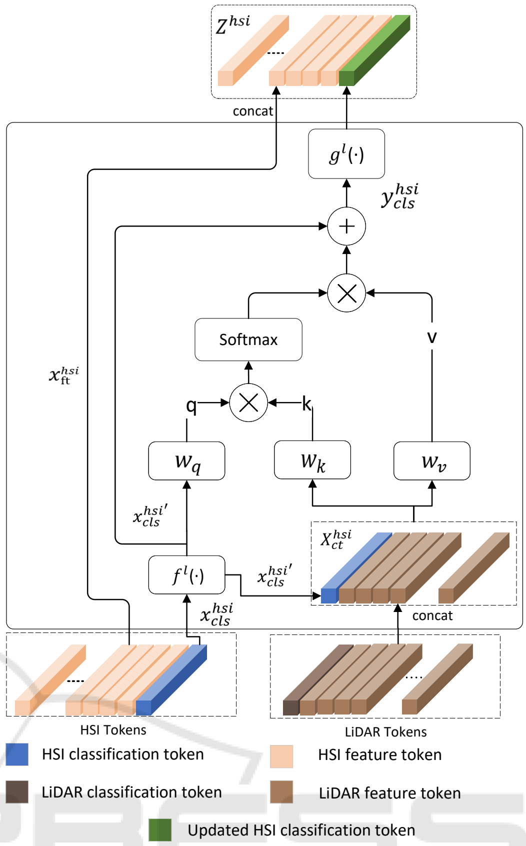

Figure 3: Internal structure of the cross-modal attention module, which jointly learns features from HSI and LiDAR data to extract complementary information.

4.1 Dataset

The Trento dataset (Rasti et al., 2017a), utilized for evaluating the proposed technique, consists of multimodal data that have HSI and LiDAR modalities. This dataset captures diverse land cover types across southern Italy, collected using the ASIA sensor for HSI and the Optech ALTM 3100EA sensor for LiDAR. The HSI data contains 63 spectral bands spanning the electromagnetic spectrum from 0.42 to 0.99 micrometers. The dataset is categorized into six distinct classes, with both HSI and LiDAR data featuring a spatial resolution of 166 × 166. Detailed distributions of the training and testing samples used to assess the proposed technique are presented in Table 1.

Table 1: Description of used Trento dataset (Rasti et al., 2017a).

No	Classes	Training	Testing
1	Apple Trees	129	3905
2	Buildings	125	2778
3	Ground	105	374
4	Wood	154	8969
5	Vineyards	184	10317
6	Roads	122	3052
-	-	819	29395

4.2 Experimental Setup

The training of the proposed model was executed on a system equipped with an Intel Core i7 processor, complemented by 32GB of RAM and an 8GB GPU. Experiments were conducted using a learning rate of 0.001 and a batch size of 64, aligning with the parameters commonly adopted in similar research studies. The optimization was facilitated by the Adam optimizer, selected for its robust performance in comparable scenarios. This setup maintained a consistent learning rate and batch size throughout the experiments. The model's performance was evaluated using the cross-entropy loss function, mathematically represented in Equation 8.

$$L_{CE}(\mathbf{y},\mathbf{p}) = -\sum_{i=1}^{C} y_i \log(p_i) \tag{8}$$

where y is the one-hot encoded true label vector, p is the predicted probability distribution across C classes, y_i is the true label for class i , and p_i is the predicted probability for class i.

4.3 Classification Results

In this work, three evaluation metrics have been used to assess the performance of the proposed technique on the Trento dataset. The evaluation metrics are overall accuracy, average accuracy, and kappa. Overall accuracy evaluates the performance by considering the total correct predictions, whereas average accuracy and kappa account for class-wise correct predictions.

The results of the proposed technique are compared against CNN-based (Hong et al., 2020) (Zhang et al., 2018) and transformer-based approaches (Feng et al., 2024) (Roy et al., 2023) (Roy et al., 2024). All these techniques used data samples for training and testing, as in Table 1. The performance comparison of our proposed technique with the mentioned techniques is presented in Table 2. The table depicts the superiority of our proposed technique across all three metrics used (highlighted in the table). We repeated the experiments five times, reporting the mean and standard deviation. Figure 4 shows a boxplot that illustrates the deviation from the mean value. The boxplot indicates that overall accuracy and kappa are more stable compared to average accuracy.

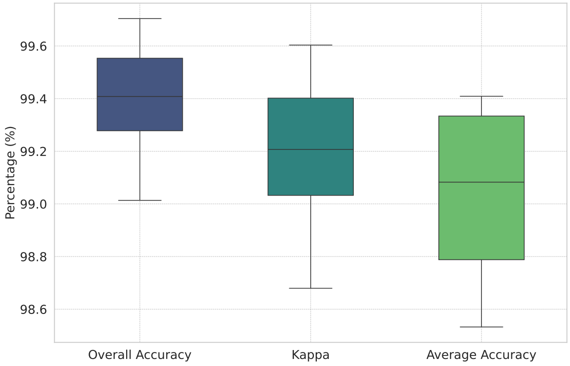

Figure 4: Boxplot showing the variability and median values of overall accuracy, kappa, and average accuracy across five experimental iterations.

The Cross-HL technique shows the second-best results in terms of overall accuracy and kappa, and slightly less average accuracy compared to PToP CNN. Furthermore, to conduct a thorough analysis, class-wise accuracy is presented in Table 3, which provides further insights into the results of the proposed technique. The class-wise accuracies of our proposed technique are consistent across all classes, showcasing its ability to learn discriminative features. The proposed technique attained the highest accuracy in two classes, namely Wood and Roads. It can be observed from the table that all other techniques show limitations in recognizing Buildings and Roads classes.

Unlike other techniques, which perform well either on Buildings or Roads class, both Cross-HL and our proposed technique exhibit nearly equal accuracy on these classes. However, our technique shows significant improvements of 3.29% for Buildings and 4.51% for Roads compared to Cross-HL. MFT, despite attaining the highest accuracy for the Buildings class, demonstrated decreased accuracy in the Roads class, reporting only 88.72%, which was the lowest among all evaluated techniques. It can be noticed that some of the other compared techniques perform well on certain classes; however, they are unable to recognize difficult classes—such as Buildings, Ground, and Roads—effectively, reducing their overall performance. The results of our proposed method can also be validated with a confusion matrix presented in Figure 5, which provides similar insights; Buildings and Roads classes are the most misclassified, likely due

Table 2: Overall performance comparison with other techniques.

Evaluation metrics	CNN-based techniques		Transformer-based techniques			
	EndNet	PToP CNN	S2EFT	MFT	Cross-HL	Ours
OA	94.17	98.34	98.45	97.76 ± 0.40	98.69 ± 0.31	**99.40** ± **0.22**
AA	93.88	97.53	97.62	95.91 ± 0.41	97.47 ± 0.30	**99.04** ± **0.33**
k	92.22	97.79	97.92	97.00 ± 0.53	98.25 ± 0.26	**99.19** ± **0.30**

Table 3: Class-wise accuracy comparison with other techniques.

Classes	CNN-based techniques		Transformer-based techniques			
	EndNet	PToP CNN	S2EFT	MFT	Cross-HL	Ours
Apple Tree	88.19	**99.60**	97.95	98.23 ± 0.38	99.32 ± 0.31	98.43 ± 0.57
Building	98.49	93.90	97.77	**99.34** ± **0.02**	95.32 ± 1.42	98.61 ± 1.03
Ground	95.19	**100**	98.40	89.84 ± 9.00	97.62 ± 0.17	99.36± 0.52
Wood	99.30	99.27	99.73	99.82 ± 0.26	99.89 ± 0.10	**100** ± **0.00**
Vineyard	91.96	100	99.50	99.93 ± 0.05	**99.97** ± **0.04**	99.74 ± 0.44
Road	90.14	97.28	92.37	88.72 ± 0.94	94.17 ± 1.36	**98.68** ± **0.67**

to similar spectral information from their same construction materials. The Apple Trees class also shows some instances of misclassification with the Ground and Vineyard classes. Woods and Vineyard classes are accurately classified.

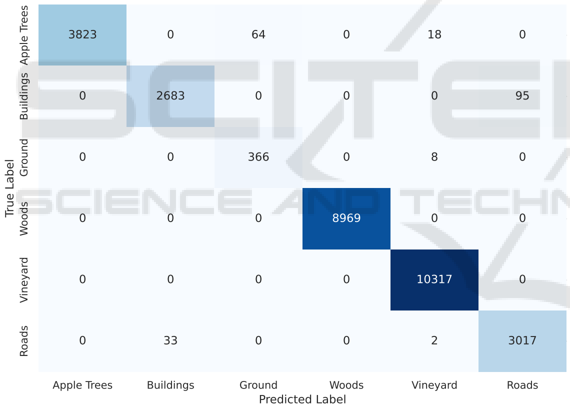

Figure 5: The confusion matrix of the proposed technique illustrates the misclassification between different classes. This matrix represents the results achieved from one of the five experimental runs, offering insight into the model's classification performance.

Moreover, we have used a t-SNE plot to visualize the predictions on the test set. It also displays the number of test samples per class with the cluster size; a larger cluster indicates a larger test sample for that particular class. The trend of misclassification can also be seen through the t-SNE plot in Figure 6, where the Buildings class (purple) overlaps with the Roads class (yellow), depicting misclassification between them. Both the confusion matrix and t-SNE plots support our results presented in Tables 2 and 3. Figure 7 visually presents the HSI and LiDAR modalities along with the ground truth. It also shows the classification map generated using the proposed technique in Figure 7(d).

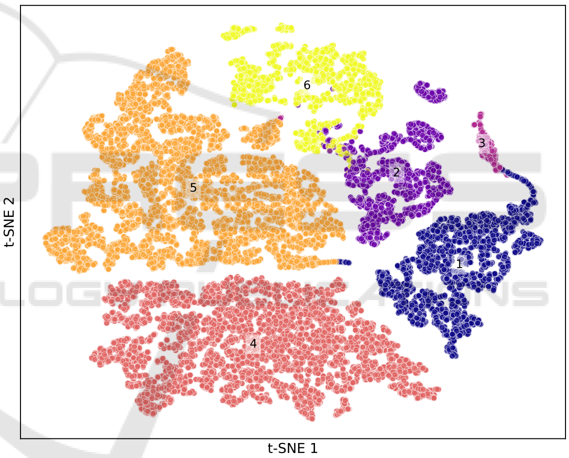

Figure 6: t-SNE visualization of predicted class distributions from the test set. Colors indicate predicted classes: Apple tree (blue), Building (purple), Ground (pink), Wood (red), Vineyard (orange), and Roads (yellow). (Best viewed in color).

4.4 Analysis of the Impact of Patch Size and Attention Heads

Several experiments were conducted to assess the impact of varying patch sizes and the number of attention heads in the transformer encoder on model performance. The patch sizes considered were 7, 9, 11, and 13. The performance based on patch size can be analyzed using a radar chart, where each axis represents a patch size, as shown in Figure 8(a). The analysis revealed that the optimal performance was achieved with a patch size of 11, as it is closest to

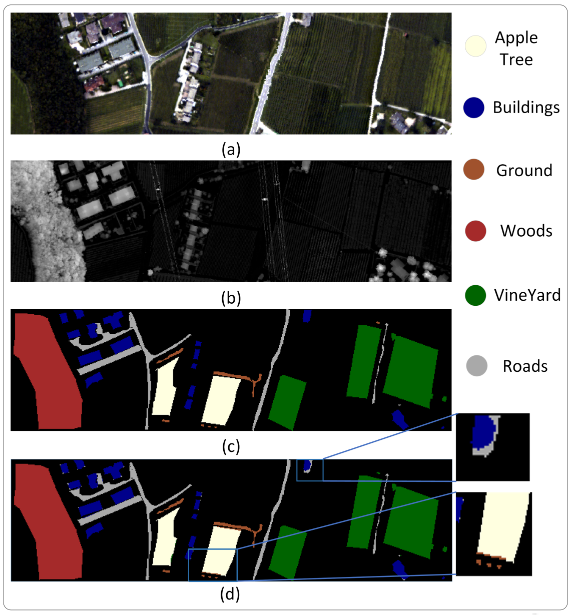

Figure 7: (a) shows the pseudo-color map of the HSI data using selected bands (20, 15, 5), (b) shows the grayscale visualization of the LiDAR data, (c) shows the ground truth available for six unique classes, (d) represents the classification map generated using the proposed technique.

the outermost edge (indicating higher values) on the radar chart for overall accuracy, average accuracy, and kappa. Similarly, optimal performance is achieved when the number of attention heads is 8, with each axis representing different attention heads, i.e., 2, 4, 6, and 8. Figure 8(b) shows that optimal performance is attained using 8 attention heads.

5 CONCLUSION

In this study, we presented a novel transformer-based technique for multimodal land use classification, utilizing HSI and LiDAR modalities. The proposed dual-stream architecture effectively extracts features from both modalities, with the cross-modal convolutional transformer demonstrating its ability to learn local and global features. The incorporation of a cross-modal attention module enables joint learning between modalities, utilizing complementary information to extract more discriminative features. The proposed method enhances classification accuracy for impactful applications in environmental monitoring, urban planning, and other areas where precise land use classification is essential.

Our experimental results demonstrate the superior performance of this technique over comparable existing methods, showcasing its potential to advance the field of remote sensing. Future work will focus on incorporating additional modalities and further improving the model to handle complex datasets, ensuring broader applicability and continued advancements in performance.

REFERENCES

Chen, C.-F. R., Fan, Q., and Panda, R. (2021). Crossvit: Cross-attention multi-scale vision transformer for image classification. In *Proceedings of the IEEE/CVF international conference on computer vision*, pages 357–366.

Ding, K., Lu, T., Fu, W., Li, S., and Ma, F. (2022). Global–local transformer network for hsi and lidar data joint classification. *IEEE Transactions on Geoscience and Remote Sensing*, 60:1–13.

Ding, Z., Zhou, D., Li, H., Hou, R., and Liu, Y. (2021). Siamese networks and multi-scale local extrema scheme for multimodal brain medical image fusion. *Biomedical Signal Processing and Control*, 68:102697.

Du, X., Zheng, X., Lu, X., and Doudkin, A. A. (2021). Multisource remote sensing data classification with graph fusion network. *IEEE Transactions on Geoscience and Remote Sensing*, 59(12):10062–10072.

Fan, Y., Qian, Y., Qin, Y., Wan, Y., Gong, W., Chu, Z., and Liu, H. (2022). Mslaenet: Multiscale learning and attention enhancement network for fusion classification of hyperspectral and lidar data. *IEEE Journal of Selected Topics in Applied Earth Observations and Remote Sensing*, 15:10041–10054.

Feng, M., Gao, F., Fang, J., and Dong, J. (2021). Hyperspectral and lidar data classification based on linear self-attention. In *2021 IEEE International Geoscience and Remote Sensing Symposium IGARSS*, pages 2401–2404.

Feng, Q., Zhu, D., Yang, J., and Li, B. (2019). Multisource hyperspectral and lidar data fusion for urban land-use mapping based on a modified two-branch convolutional neural network. *ISPRS International Journal of Geo-Information*, 8(1):28.

Feng, Y., Zhu, J., Song, R., and Wang, X. (2024). S2eft: Spectral-spatial-elevation fusion transformer for hyperspectral image and lidar classification. *Knowledge-Based Systems*, 283:111190.

Ghamisi, P., Yokoya, N., Li, J., Liao, W., Liu, S., Plaza, J., Rasti, B., and Plaza, A. (2017). Advances in hyperspectral image and signal processing: A comprehensive overview of the state of the art. *IEEE Geoscience and Remote Sensing Magazine*, 5(4):37–78.

Gulati, A., Qin, J., Chiu, C.-C., Parmar, N., Zhang, Y., Yu, J., Han, W., Wang, S., Zhang, Z., Wu, Y., et al. (2020). Conformer: Convolution-augmented transformer for speech recognition. *arXiv preprint arXiv:2005.08100.*

Gómez-Chova, L., Tuia, D., Moser, G., and Camps-Valls, G. (2015). Multimodal classification of remote sensing images: A review and future directions. *Proceedings of the IEEE*, 103(9):1560–1584.

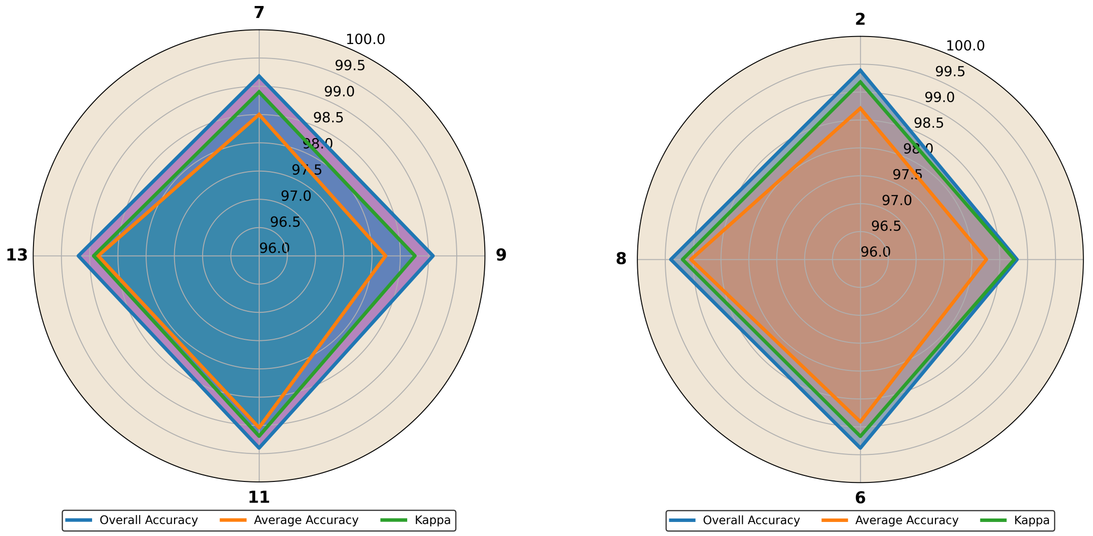

(a) (b)

Figure 8: Radar charts depicting the analysis of model performance: (a) shows the impact of patch size, while (b) illustrates the effect of the number of attention heads. The chart highlights optimal performance at a patch size of 11 and 8 attention heads. (Best viewed in color).

Hermessi, H., Mourali, O., and Zagrouba, E. (2021). Multimodal medical image fusion review: Theoretical background and recent advances. *Signal Processing*, 183:108036.

Hong, D., Gao, L., Hang, R., Zhang, B., and Chanussot, J. (2020). Deep encoder–decoder networks for classification of hyperspectral and lidar data. *IEEE Geoscience and Remote Sensing Letters*, 19:1–5.

Hong, D., Han, Z., Yao, J., Gao, L., Zhang, B., Plaza, A., and Chanussot, J. (2021). Spectralformer: Rethinking hyperspectral image classification with transformers. *IEEE Transactions on Geoscience and Remote Sensing*, 60:1–15.

Hong, D., Han, Z., Yao, J., Gao, L., Zhang, B., Plaza, A., and Chanussot, J. (2022). Spectralformer: Rethinking hyperspectral image classification with transformers. *IEEE Transactions on Geoscience and Remote Sensing*, 60:1–15.

Jia, S., Zhan, Z., Zhang, M., Xu, M., Huang, Q., Zhou, J., and Jia, X. (2021). Multiple feature-based superpixel-level decision fusion for hyperspectral and lidar data classification. *IEEE Transactions on Geoscience and Remote Sensing*, 59(2):1437–1452.

Khotimah, W. N., Bennamoun, M., Boussaid, F., Xu, L., Edwards, D., and Sohel, F. (2023). Mce-st: Classifying crop stress using hyperspectral data with a multiscale conformer encoder and spectral-based tokens. *International Journal of Applied Earth Observation and Geoinformation*, 118:103286.

Li, J., Ma, Y., Song, R., Xi, B., Hong, D., and Du, Q. (2022). A triplet semisupervised deep network for fusion classification of hyperspectral and lidar data. *IEEE Transactions on Geoscience and Remote Sensing*, 60:1–13.

Liao, W., Pižurica, A., Bellens, R., Gautama, S., and Philips, W. (2014). Generalized graph-based fusion of hyperspectral and lidar data using morphological features. *IEEE Geoscience and Remote Sensing Letters*, 12(3):552–556.

Mohla, S., Pande, S., Banerjee, B., and Chaudhuri, S. (2020). Fusatnet: Dual attention based spectrospatial multimodal fusion network for hyperspectral and lidar classification. In *Proceedings of the IEEE/CVF Conference on Computer Vision and Pattern Recognition Workshops*, pages 92–93.

Ni, K., Wang, D., Zheng, Z., and Wang, P. (2024). Mhst: Multiscale head selection transformer for hyperspectral and lidar classification. *IEEE Journal of Selected Topics in Applied Earth Observations and Remote Sensing*.

Rasti, B. and Ghamisi, P. (2020). Remote sensing image classification using subspace sensor fusion. *Information Fusion*, 64:121–130.

Rasti, B., Ghamisi, P., and Gloaguen, R. (2017a). Hyperspectral and lidar fusion using extinction profiles and total variation component analysis. *IEEE Transactions on Geoscience and Remote Sensing*, 55(7):3997–4007.

Rasti, B., Ghamisi, P., Plaza, J., and Plaza, A. (2017b). Fusion of hyperspectral and lidar data using sparse and low-rank component analysis. *IEEE Transactions on Geoscience and Remote Sensing*, 55(11):6354–6365.

Roy, S. K., Deria, A., Hong, D., Rasti, B., Plaza, A., and Chanussot, J. (2023). Multimodal fusion transformer for remote sensing image classification. *IEEE Transactions on Geoscience and Remote Sensing*, 61:1–20.

Roy, S. K., Sukul, A., Jamali, A., Haut, J. M., and Ghamisi, P. (2024). Cross hyperspectral and lidar attention transformer: An extended self-attention for land use and land cover classification. *IEEE Transactions on Geoscience and Remote Sensing*.

Tang, W., He, F., Liu, Y., and Duan, Y. (2022). Matr: Multimodal medical image fusion via multiscale adaptive transformer. *IEEE Transactions on Image Processing*, 31:5134–5149.

Vaswani, A. (2017). Attention is all you need. *Advances in Neural Information Processing Systems*.

Wang, X., Feng, Y., Song, R., Mu, Z., and Song, C. (2022). Multi-attentive hierarchical dense fusion net for fusion classification of hyperspectral and lidar data. *Information Fusion*, 82:1–18.

Wu, X., Hong, D., and Chanussot, J. (2021). Convolutional neural networks for multimodal remote sensing data classification. *IEEE Transactions on Geoscience and Remote Sensing*, 60:1–10.

Xue, Z., Tan, X., Yu, X., Liu, B., Yu, A., and Zhang, P. (2022). Deep hierarchical vision transformer for hyperspectral and lidar data classification. *IEEE Transactions on Image Processing*, 31:3095–3110.

Xue, Z., Yu, X., Tan, X., Liu, B., Yu, A., and Wei, X. (2021). Multiscale deep learning network with self-calibrated convolution for hyperspectral and lidar data collaborative classification. *IEEE Transactions on Geoscience and Remote Sensing*, 60:1–16.

Yang, B., Wang, X., Xing, Y., Cheng, C., Jiang, W., and Feng, Q. (2024). Modality fusion vision transformer for hyperspectral and lidar data collaborative classification. *IEEE Journal of Selected Topics in Applied Earth Observations and Remote Sensing*.

Yu, Y., Jiang, T., Gao, J., Guan, H., Li, D., Gao, S., Tang, E., Wang, W., Tang, P., and Li, J. (2022). Capvit: Cross-context capsule vision transformers for land cover classification with airborne multispectral lidar data. *International Journal of Applied Earth Observation and Geoinformation*, 111:102837.

Zhang, M., Gao, F., Zhang, T., Gan, Y., Dong, J., and Yu, H. (2023). Attention fusion of transformer-based and scale-based method for hyperspectral and lidar joint classification. *Remote Sensing*, 15(3):650.

Zhang, M., Li, W., Du, Q., Gao, L., and Zhang, B. (2018). Feature extraction for classification of hyperspectral and lidar data using patch-to-patch cnn. *IEEE transactions on cybernetics*, 50(1):100–111.

Zhang, M., Li, W., Tao, R., Li, H., and Du, Q. (2021). Information fusion for classification of hyperspectral and lidar data using ip-cnn. *IEEE Transactions on Geoscience and Remote Sensing*, 60:1–12.

Zhang, Y., Peng, Y., Tu, B., and Liu, Y. (2022). Local information interaction transformer for hyperspectral and lidar data classification. *IEEE Journal of Selected Topics in Applied Earth Observations and Remote Sensing*, 16:1130–1143.

Zhao, G., Ye, Q., Sun, L., Wu, Z., Pan, C., and Jeon, B. (2022). Joint classification of hyperspectral and lidar data using a hierarchical cnn and transformer. *IEEE Transactions on Geoscience and Remote Sensing*, 61:1–16.